Electronic Supplementary Material (ESI)

Intrareticular electron coupling pathway driven electrochemiluminescence in hydrogen-bonded organic frameworks

Hanlin Hou,[‡,a] Yunlei Wang,[‡,b] Yufei Wang,[a] Rengan Luo,[a] Da Zhu,[a] Jun Zhou,[*,a] Xiaojun Wu,[*,b] Huangxian Ju[a] and Jianping Lei[*,a]

a.   State Key Laboratory of Analytical Chemistry for Life Science, School of Chemistry and Chemical Engineering, Nanjing University, Nanjing 210023, China E-mail: jun.zhou@nju.edu.cn, jpl@nju.edu.cn.
b.   School of Chemistry and Materials Sciences, Synergetic Innovation of Quantum Information and Quantum Technology, CAS Key Laboratory of Materials for Energy Conversion, CAS Centre for Excellence in Nanoscience, University of Science and Technology of China, Hefei 230026, China E-mail: xjwu@ustc.edu.cn.

Table of Contents

Experimental Procedures

Materials and reagents

Potassium chloride (KCl, 99%), tri-n-propylamine (TPrA, >99%), triethylamine (TEtA, >99%) and 2-dibutyaminoethanol (DBAE, >99%) were purchased from Aladdin. 1,3,6,8-tetracarboxy pyrene (TCPY, 99%) and 1,3,6,8-tetra(4-carboxylphenyl)pyrene (TCPPY, 99%) were purchased from CHEMSOON Co. Ltd. (Shanghai, China). Magnesium chloride hexahydrate ($MgCl_2 \cdot 6H_2O$, 99%) and N,N-dimethylformamide (DMF) were purchased from Tensus Biotech Co., Ltd. (Shanghai, China). Potassium ferricyanide ($K_3Fe(CN)_6$), potassium hexacyanoferrate ($K_4Fe(CN)_6$), 1,4-dioxane (99.5%) and methanol (MeOH) were bought from Nanjing Chemical Reagent Co., Ltd. Pyrene (98%) was purchased from Heowns (Tianjin, China). Tetrahydrofuran (THF, 99%), Sodium phosphate monobasic dihydrate ($NaH_2PO_4 \cdot 2H_2O$) and sodium phosphate dibasic dodecahydrate ($Na_2HPO_4 \cdot 12H_2O$) were obtain from Sinopharm Chemical Reagent Co., Ltd. (Shanghai, China). Phosphate buffer solution (PBS, 0.1 M) was prepared by mixing stock solutions of NaH_2PO_4 and Na_2HPO_4. Ultrapure water obtained from Millipore water purification system (≥ 18 MΩ cm, MilliQ, Millipore) was used in all assays. All chemicals were of analytical grade.

Apparatus

Powder X-ray diffraction (PXRD) patterns were collected on Bruker D8 Advance employing Cu Kα line focused radiation ($\lambda = 1.54178$ Å) at 40 kV, 40 mA powder with 0.1 s per step. Samples were rotated as diffraction data were collected using a continuous 2θ scan from 3-50°. Transmission electron microscopic (TEM) images were recorded on a JEM-2800 high resolution transmission electron microscope (JEOL, Japan), operated at an acceleration voltage of 200 kV. The scanning electron microscopic (SEM) images were obtained from a JSM-7800F scanning electron microscope (JEOL, Japan). Photoluminescence (PL) spectra were measured on FLS-980 fluorescence spectrophotometer (Edinburgh Instrument., U.K.) using a quartz cell. Ultraviolet and visible diffuse reflectance spectra (UV-Vis DRS) were obtained on a UV-3600 UV-Vis-NIR spectrophotometer (Shimadzu Co., Japan) in aS3 diffuse reflection mode. Fourier transform infrared (FT-IR) spectra were taken with a spectrum on a FTIR spectrophotometer (Nicolet 6700, USA) at room temperature in ATR mode. The analysis of thermal stability was performed on a thermogravimetric (TG) instrument (Netzchen, STA449F3) in the range 25-700 °C under a nitrogen atmosphere with a flow rate of 10 mL min⁻¹ and a heating rate of 10 °C min⁻¹, and the specimen mass was about 10 mg. Solution ¹H NMR spectra were collected on a 400 MHz Bruker Avance III system. The ultraviolet photoelectron spectroscopy (UPS) was measured using ESCALAB250Xi instrument with a monochromatic He I light source (21.22 eV). Electrochemical impedance spectroscopic (EIS) measurements were performed on a Parstat MC 1000 electrochemical

workstation (Princeton, USA) in 0.1 M KCl aqueous solution containing 5 mM $K_3Fe(CN)_6$/$K_4Fe(CN)_6$ (1:1). Optical photographs of single crystals were obtained from U-LH100HGAPO (OLYMPUS, Japan). Zeta potential analyses were conducted on Nano-Z Zetasizer (Malvern, UK). Surface areas were measured by nitrogen sorption at 77.3 K. The powder samples were degassed under vacuum at 80 °C for 12 h. Isotherm measurements were performed using a JW-BK200B volumetric gas sorption instrument equipped with nitrogen containers.

Cyclic voltammetry

Cyclic voltammetry (CV), step pulse (SP) and constant potential electrolysis were carried out with a CHI-630D electrochemical workstation (CHI Instruments Inc., China). All anode and cathode studies were carried out in the potential range from 0.0 V to +1.5 V and 0.0 V to -2.2 V, respectively, with the conventional three-electrode system, which contains a glassy carbon electrode (GCE, d = 5 mm), a platinum wire and Ag/AgCl electrode as a working electrode, a counter electrode, and a reference electrode, respectively. Before each experiment, the GCE was polished with 0.3 mm and 0.05 mm alumina powder, followed by ultrasonic cleaning with ethanol and water three times, and then dried with a steam of high-purity nitrogen gas.

ECL spectra

The ECL spectrum was obtained by a self-made ECL spectrum analyzer consisting of a CHI-660D electrochemical workstation and a FLS-980 fluorescence spectrophotometer. After 200 μL of 1.0 mg mL^{-1} HOF-101 was coated at carbon/ITO electrode, the modified electrode was immersed in 0.1 M PBS containing 0.1 M KNO_3 and 20 mM TPrA by applying a constant potential of +1.3 V for 120 s.

ECL imaging

ECL imaging is obtained by a multi-color ECL imaging system equipped with focus lens (EF 50 mm f/1.2 L USM, Canon) and Retiga R6 color scientific CCD camera (QImaging, Canada) in a dark box. A classical three-electrode system is adopted, with indium tin oxide (ITO) as the working electrode (100 × 100 × 1.1 mm), 2 μL of 1.0 mg mL^{-1} HOF-101 dispersion is dropped into the surface pore array, platinum wire as counter electrode and Ag/AgCl (saturated) as the reference electrode. A constant potential of +1.1 V was applied in 0.1 M PBS containing 0.1 M KCl and 20 mM TPrA, and the exposure time was 20 s.

Preparation of HOF-101 and HOF-100 powder
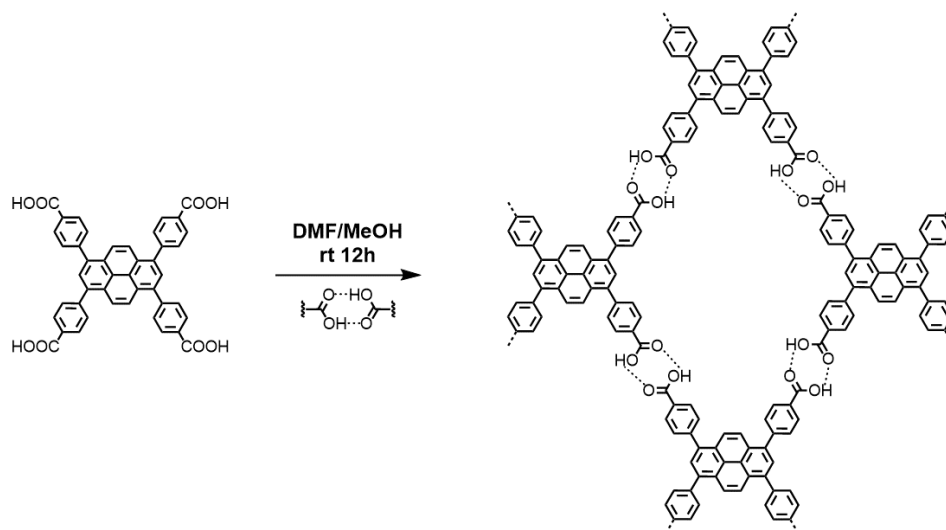
TCPPY (150 mg, 0.225 mmol) was dissolved in 22.5 mL of DMF, and then 90 mL MeOH was added and stirred for 1 min. The mixture stands at room temperature for 12 h to afford yellow block crystals of HOF-101 (Yield: 81.4%).
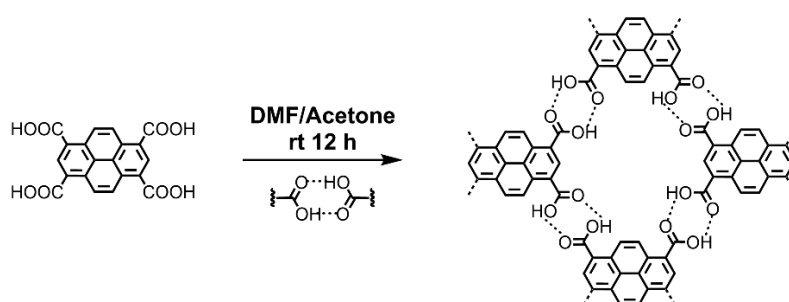
TCPY (200 mg, 0.529 mmol) was dissolved in 10 mL of DMF under heating at 120 °C for 30 min to get a clear solution. After cooling down to room temperature, the solution was poured into 160 mL of acetone under stirring (400 rpm) within 1 min. The suspension was kept stirring for 12 h and isolated by centrifugation at 8000 rpm for 5 min. The obtained brown powder was further washed with acetone (2 × 45 mL), and then dried in at room temperature (Yield: 63.8%).

Preparation of Mg-MOF

The synthesis of Mg-MOF was improved on the previously reported method.[1] A mixture of anhydrous $MgCl_2·6H_2O$ (9.6 mg, 0.047 mmol), TCPPY (11.5 mg, 0.017 mmol), 4 mL of dioxane/water/DMF (1/1/2) mixed solvents, and 25 μL of hydrochloric acid (1.0 M) was vacuum sealed into a spherical glass tube (10 mL) and heated at 90 °C for 72 h. After the mixture was cooled to room temperature at a rate of 5 °C h^{-1}, yellow rod-like crystals of Mg-MOF were obtained (Yield: 73.9%).

Computational details

Density functional theory (DFT) calculations, implemented in the Vienna ab initio simulation package (VASP),[2,3] are carried out for HOFs with the projector augmented wave (PAW) pseudopotential

method and Perdew−Burke−Ernzerhof (PBE) exchange-correlation functional.[4-6] Note that DFT with PBE always underestimates the band gaps of semiconductors and thus the valence-band maximum (VBM) and conduction band-minimum (CBM) were determined with the Heyd, Scuseria, and Ernzerhof (HSE06) screened hybrid density functional theory method.[7,8] The atomic positions were optimized until the Hellmann−Feynman force acting on each atom was smaller than 0.02 eV $Å^{-1}$ and the energy convergence criteria per electronic step was 1×10^{-6} eV $atom^{-1}$. The kinetic energy cutoff for plane waves was set to 400 eV. The Brillouin zones were sampled with 0.04 $Å^{-1}$ spacing in reciprocal space by the Monkhorst−Pack scheme.[9] For 2D HOFs, a 15 Å vacuum slab above 15 Å was used in all calculations to avoid the interlayer interactions.

Crystal structures of HOFs

The symmetry group of bulk HOF-100 is P1, in which the α = 90°, β = 92.8° and γ = 90°. The lattice parameters of were a = 4.755 Å, b = 17.510 Å and c= 3.81 Å; The symmetry group of bulk HOF-101 is C2/M, in which the α = 90°, β = 85.9° and γ = 90°. The lattice parameters of were a = 3.809 Å, b = 24.159 Å and c= 29.359 Å. The bulk HOFs were used to simulate the XRD pattern and 2D HOFs which contain two layers were used to calculate the energy levels. The unit-cell of bulk and 2D HOF-100 consists of 40 carbon atoms (C), 20 hydrogen atoms (H) and 16 oxygen atoms (O). The unit-cell of bulk and 2D HOF-101 consists of 88 carbon atoms (C), 52 hydrogen atoms (H) and 16 oxygen atoms (O).

Electronic structures of HOFs

2D HOF-100 and HOF-101 were calculated to be a semiconductor at the HSE06 level with a bandgap of 2.48 eV and 2.32 eV, respectively. The work function of 2D HOF-100 was calculated to be 2.33 eV. VBM and CBM locate at -7.23 eV and -4.75 eV, respectively. The work function of 2D HOF-101 was calculated to be 2.10 eV. VBM and CBM locate at -5.54 eV and -3.22 eV, respectively. Besides, the TCPY and TCPPY molecules were calculated to be a semiconductor with a bandgap of 2.80 eV and 2.63 eV, respectively. VBM and CBM for TCPY and TCPPY locate at -6.33 eV and -3.53 eV, and -5.68 eV and -3.05 eV, respectively.

Ground and excited states of HOF-101 and HOF-100 fragments

The HOF-101 and HOF-100 fragments were calculated using Gaussian 16 program package,[10] and their ground and 1st excited states have been simulated with B3LYP (Becke's 3-parameter hybrid density exchange functional with the Lee, Yang, and Parr correlation functional) by means of DFT and time-dependent density functional theory (TDDFT), respectively.[11] The basis set was selected to be 6-31G. We select two vertically stacked molecules to calculate the orbital distribution. The number of HOMO and LUMO for HOF-101 and HOF-100 fragments under 1st excited states is 354 and 355, and 194 and 195, respectively.
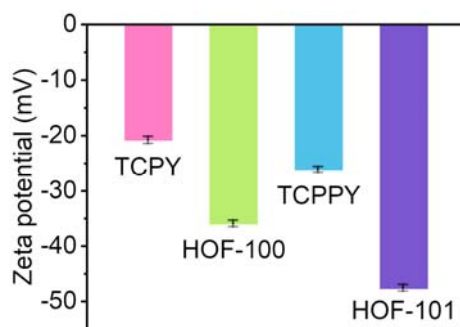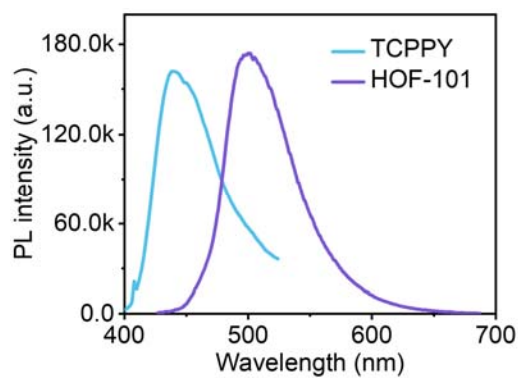
Supporting Figures
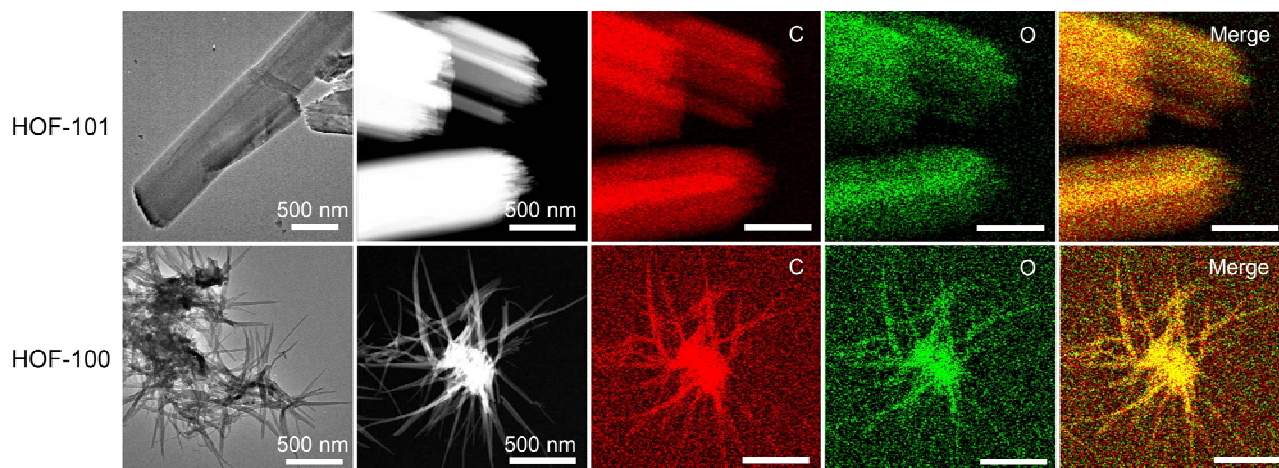
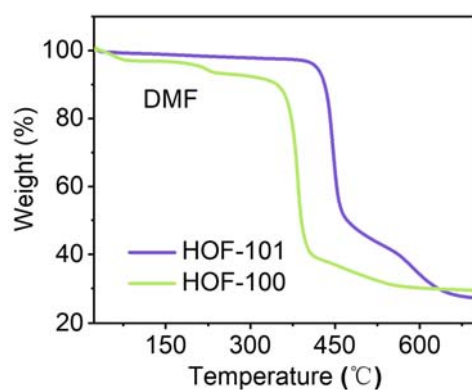**Fig. S1** TEM and mapping images of HOF-101 and HOF-100.
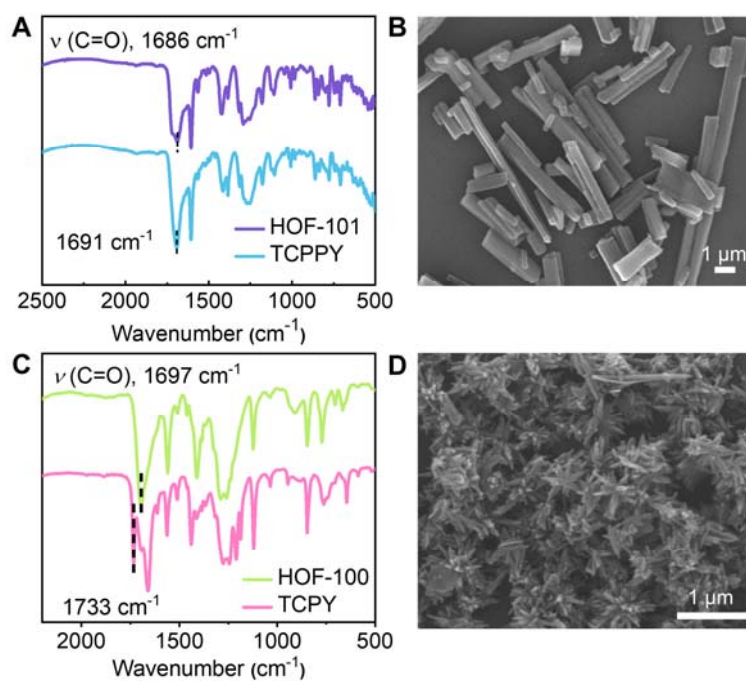
Fig. S2 FT-IR spectra of (A) HOF-101 and TCPPY, and (C) HOF-100 and TCPY. SEM images of (B) HOF-101 and (D) HOF-100.
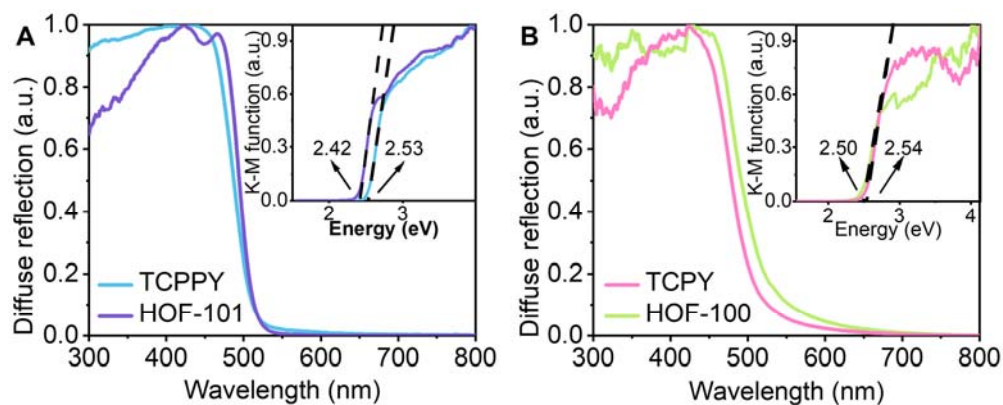

Fig. S3 Zeta potentials of HOF-101, HOF-100, TCPPY and TCPY.

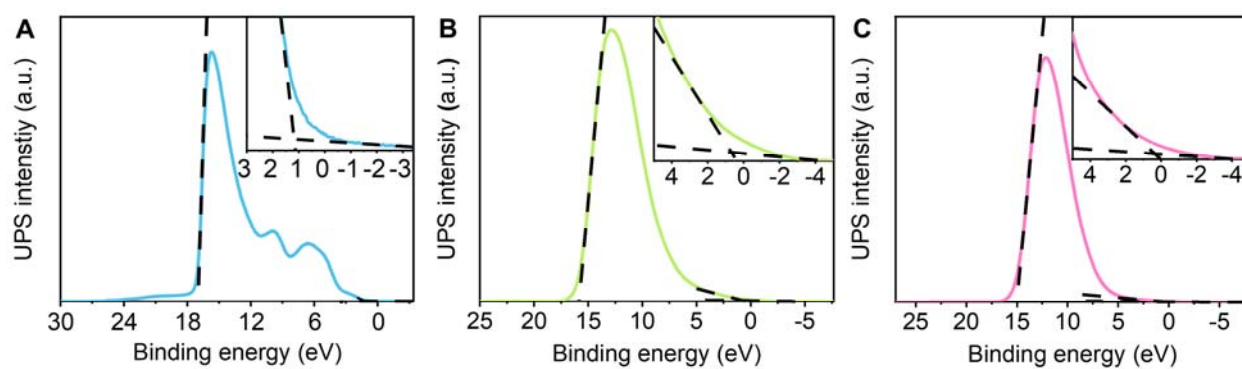**Fig. S4** PL spectra of HOF-101 and TCPPY in aqueous medium.

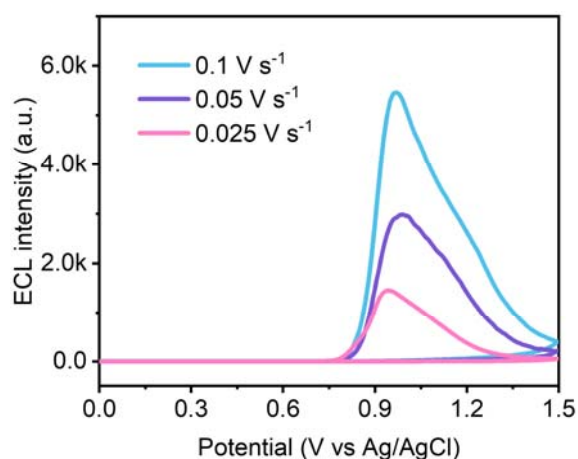**Fig. S5** Thermogravimetric analysis of HOF-101 and HOF-100.

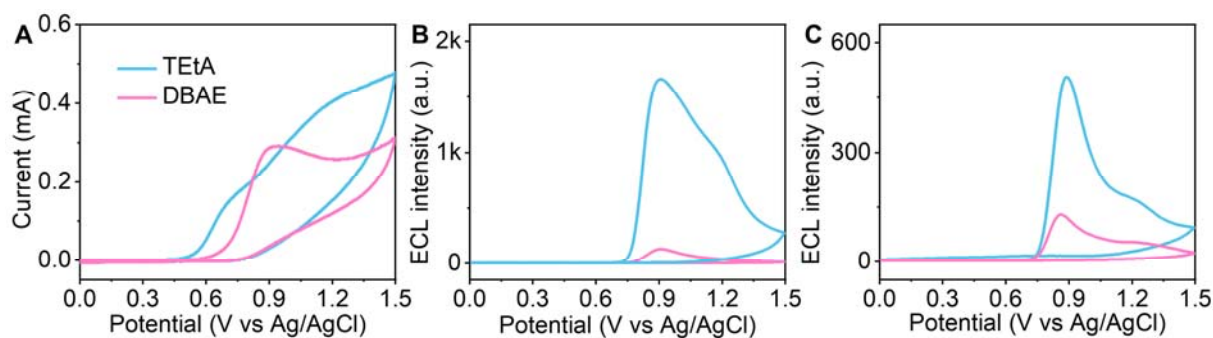**Fig. S6** UV-vis DRS and band gap energy (inset) of (A) HOF-101 and TCPPY, and (B) HOF-100 and TCPY.

**Fig. S7** UPS spectra of (A) TCPPY, (B) HOF-100 and (C) TCPY.

Fig. S8 ECL curves of HOF-101 modified GCEs under different scan rates in 0.1 M PBS containing 20 mM TPrA (PMT = 400 V).


Fig. S9 (A) CV curves of bare GCEs, and ECL curves of (B) HOF-101 and (C) TCPPY modified GCEs in 0.1 M PBS containing 20 mM TEtA (blue) and DBAE (pink) co-reactants (PMT = 400 V).
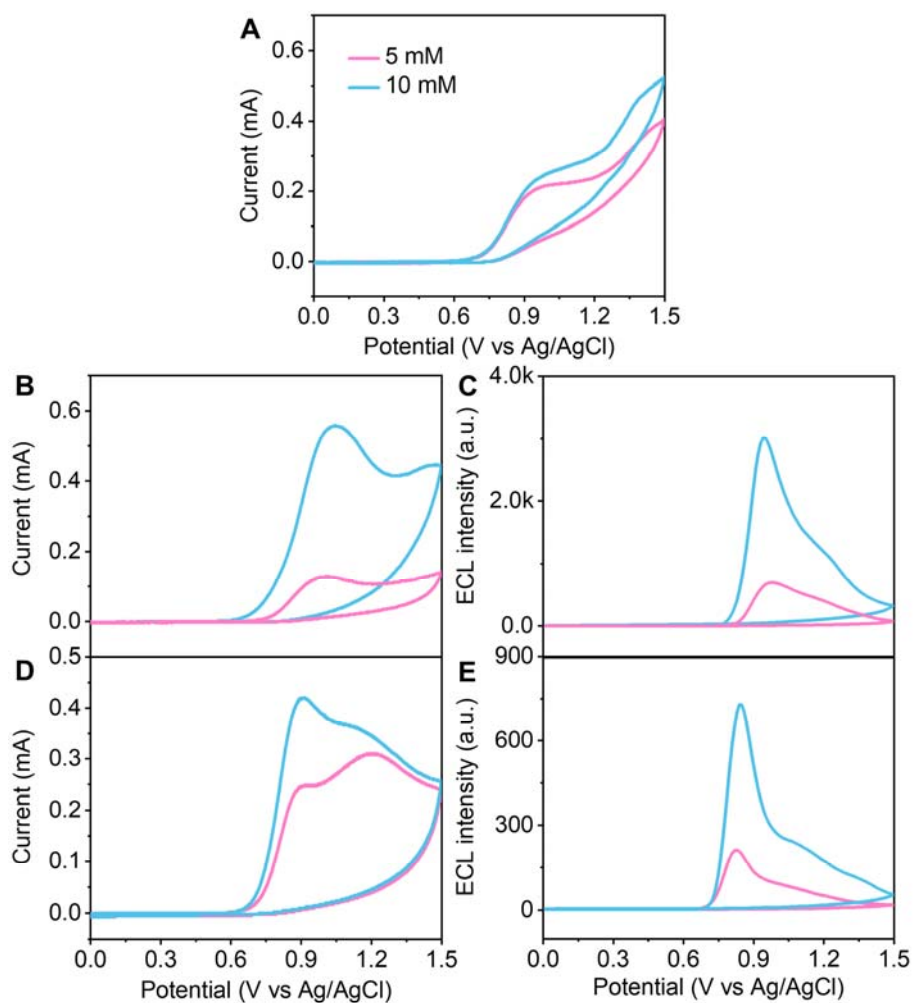
Fig. S10 (A) CV curves of bare GCEs, (B) CV and (C) ECL curves of HOF-101 modified GCEs, and (D) CV and (E) ECL curves of TCPPY modified GCEs in 0.1 M PBS containing 5.0 mM (pink), and 10 mM (blue) TPrA (PMT = 400 V).
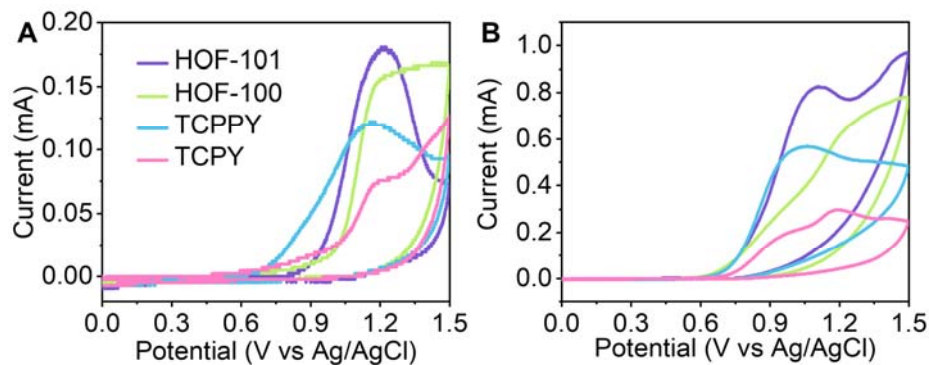

Fig. S11 CV curves of HOF-101, HOF-100, TCPPY and TCPY modified GCEs in 0.1 M PBS (A) without and (B) with 20 mM TPrA.
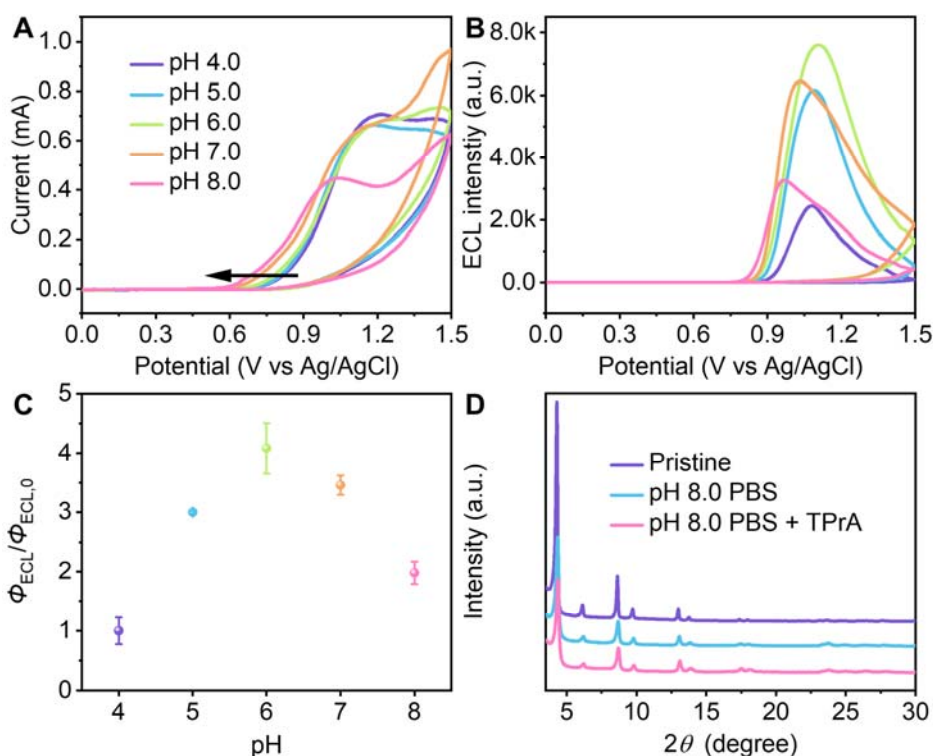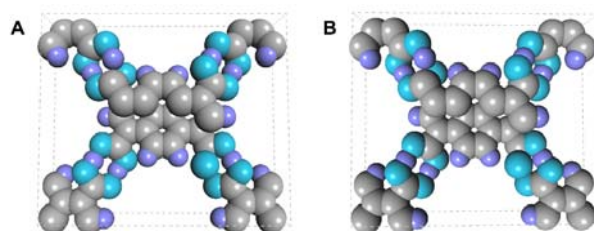
Fig. S12 (A) CV and (B) ECL curves of HOF-101 modified GCEs in PBS containing 20 mM TPrA with different pHs (PMT = 400 V). (C) Dependence of the relative ECL efficiencies ($\Phi_{ECL}/\Phi_{ECL,0}$) on pHs. Φ_{ECL} and $\Phi_{ECL,0}$ represent the ECL efficiencies of HOF-101 in given pHs and pH 4.0, respectively. (D) XRD patterns of HOF-101 powder before (purple) and after immersing in pH 8.0 PBS (bule) and pH 8.0 PBS + 20 mM TPrA (pink) for 1.0 h.
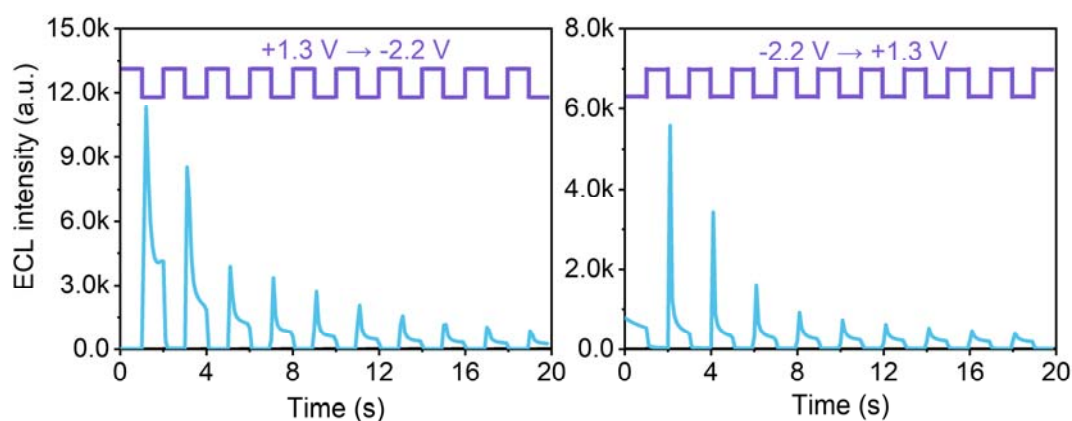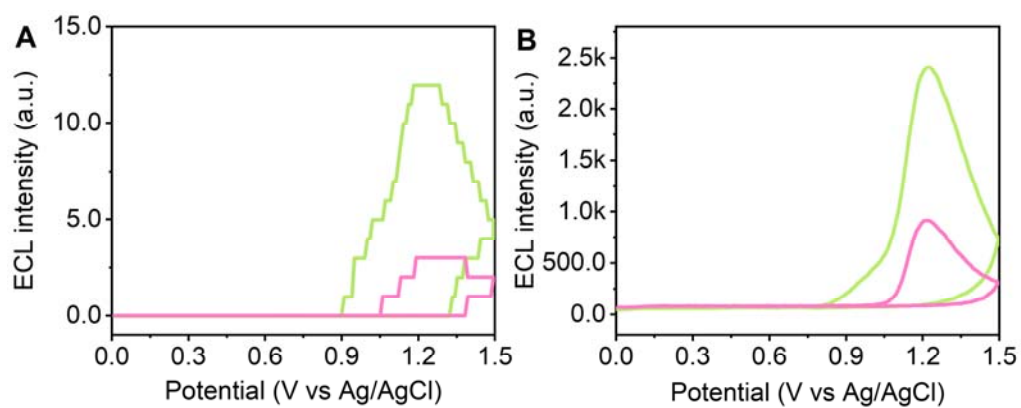

Fig. S13 ECL transients of HOF-101 modified GCEs by SP from +1.30 V to − 2.20 V (left) and from −2.20 V to +1.30 V (right) in 0.10 M PBS (PMT=400 V).
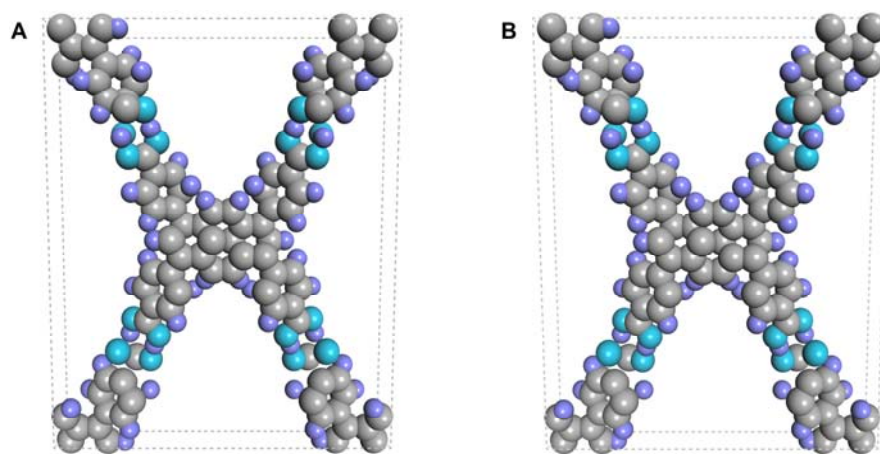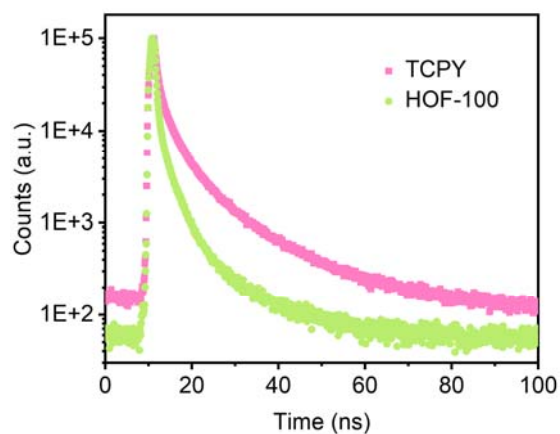
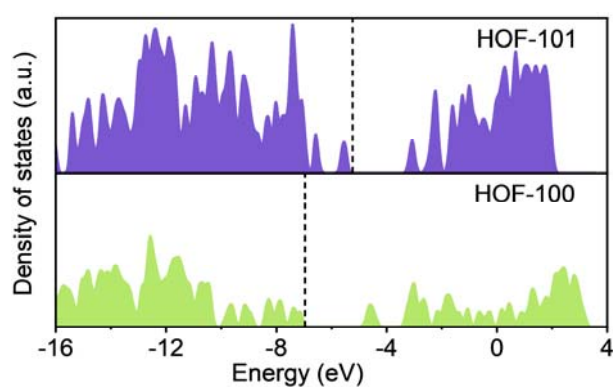**Fig. S14** (A) Electron- and (B) hole-doped 2D HOF-101 structures.

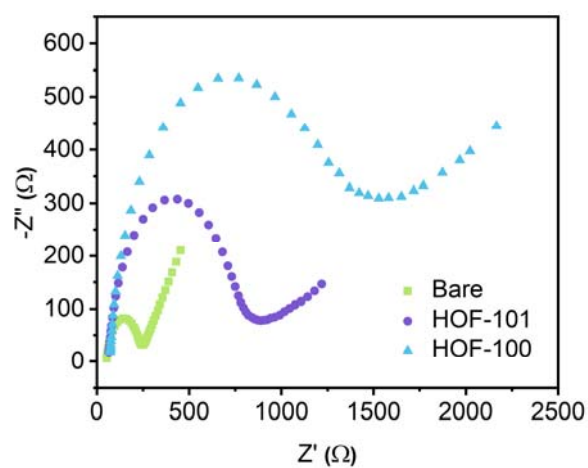**Fig. S15** (A) Electron- and (B) hole-doped 2D HOF-100 structures.

Fig. S16 ECL curves of HOF-100 (green) and TCPY (pink) modified GCEs in 0.1 M PBS containing 20 mM TPrA at (A) PMT = 400 V, and (B) PMT = 700 V.
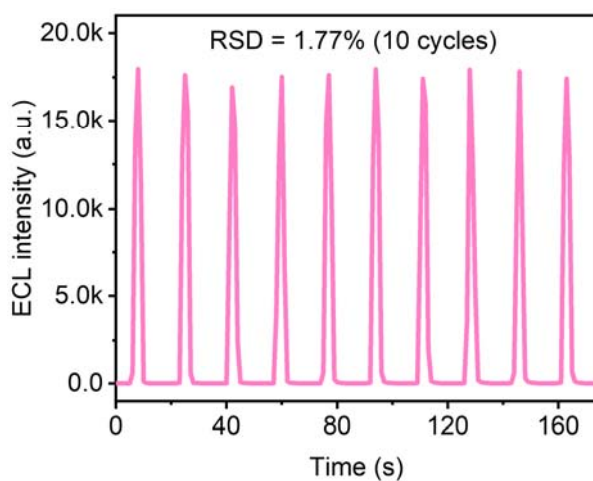
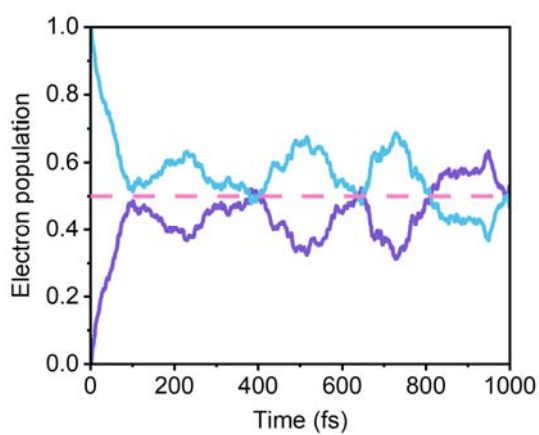**Fig. S17** TCSPC traces of solid state TCPY and HOF-100.

Fig. S18 Density of states of HOF-101 and HOF-100.

Fig. S19 EIS of bare GCE, HOF-101 and HOF-100 modified GCEs in 5.0 mM [Fe(CN)$_6$]$^{3-}$/$^{4-}$ (1:1) solution containing 0.1 M KCl.
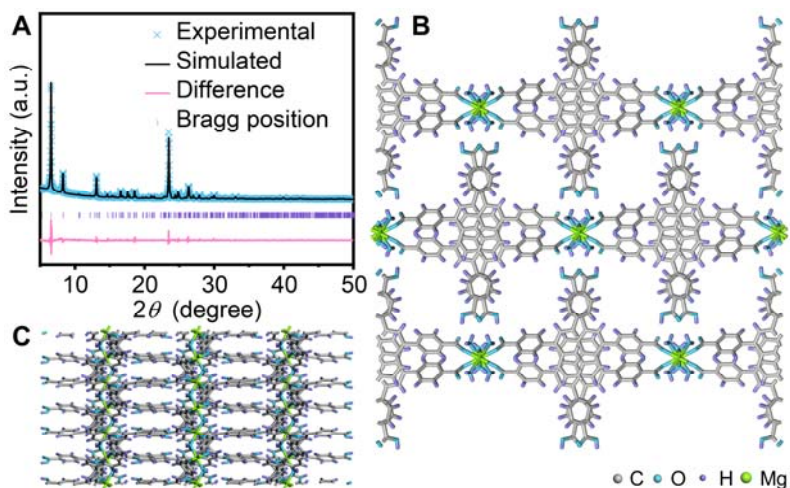
Fig. S20 Continuous ECL signals between 0 V and +1.0 V of HOF-101 modified GCE in 0.10 M PBS containing 20 mM TPrA (PMT = 500 V).
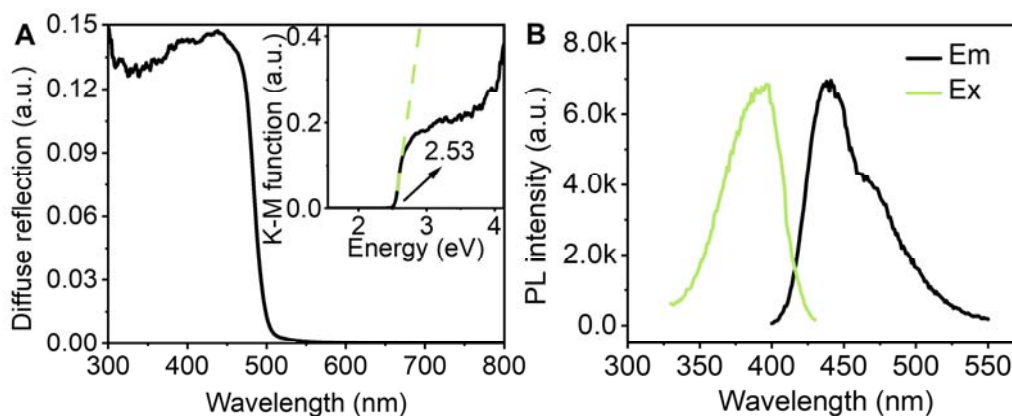

Fig. S21 Time-dependent electron population at 300 K for HOF-101.
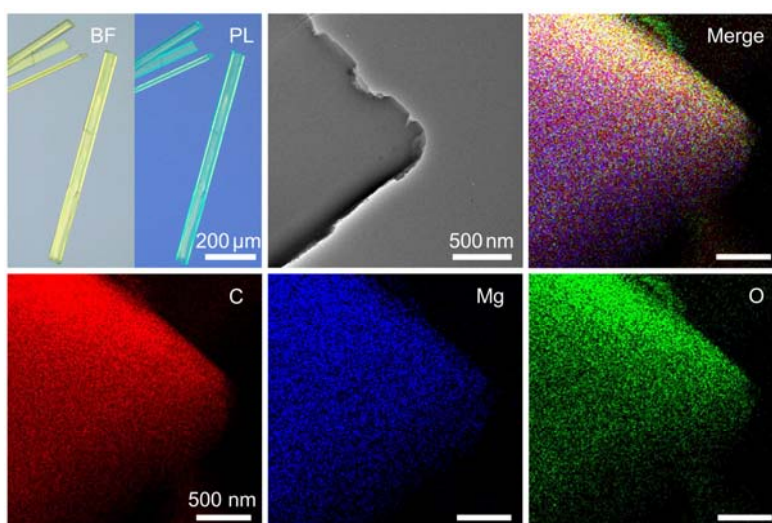
Fig. S22 Single crystal optical photograph, TEM, and mapping images of Mg-MOF.

Fig. S23 (A) Pawley-refined and experimental PXRD patterns of Mg-MOF. Crystal structure of Mg-MOF in (B) top and (C) side views.

Fig. S24 (A) UV-vis DRS and band gap energy (inset), and (B) fluorescence spectra of Mg-MOF.
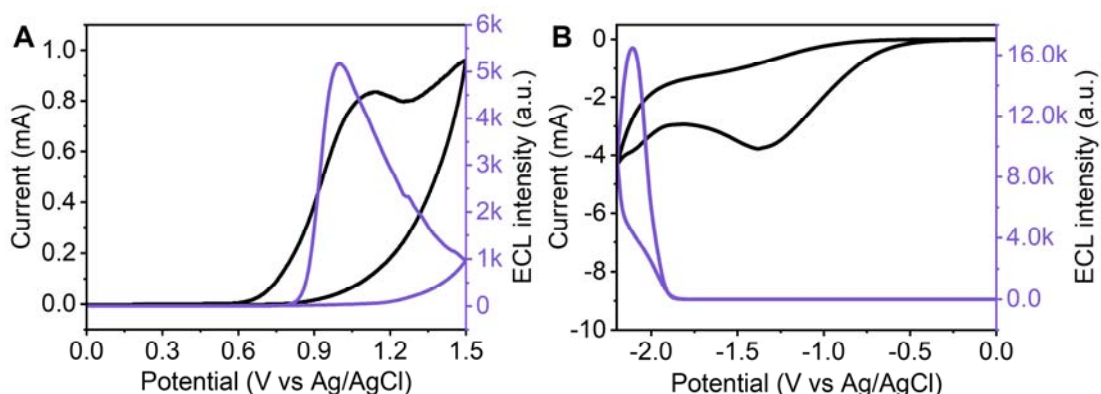
Fig. S25 (A) CV (black) and anodic ECL (purple) curves of HOF-101 and MgCl$_2$ mixture modified GCEs in 0.1 M PBS with 20 mM TPrA (PMT = 400 V). (B) CV (black) and cathodic ECL (purple) curves of HOF-101 and MgCl$_2$ mixture modified GCEs in 0.1 M PBS with 0.1 M K$_2$S$_2$O$_8$ (PMT = 250 V).
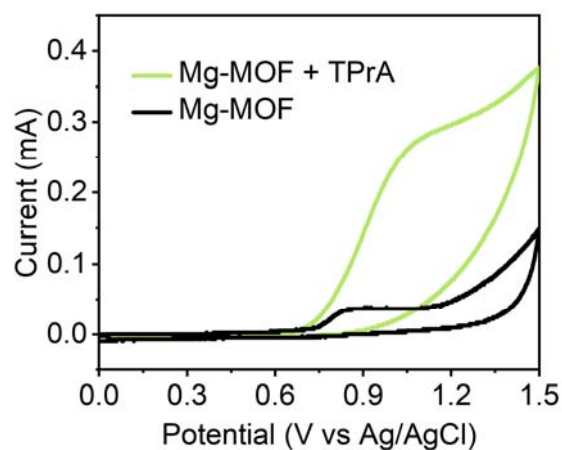
Fig. S26 CV curves of Mg-MOF modified GCEs in 0.1 M PBS without (dark) and with (green) 20 mM TPrA.
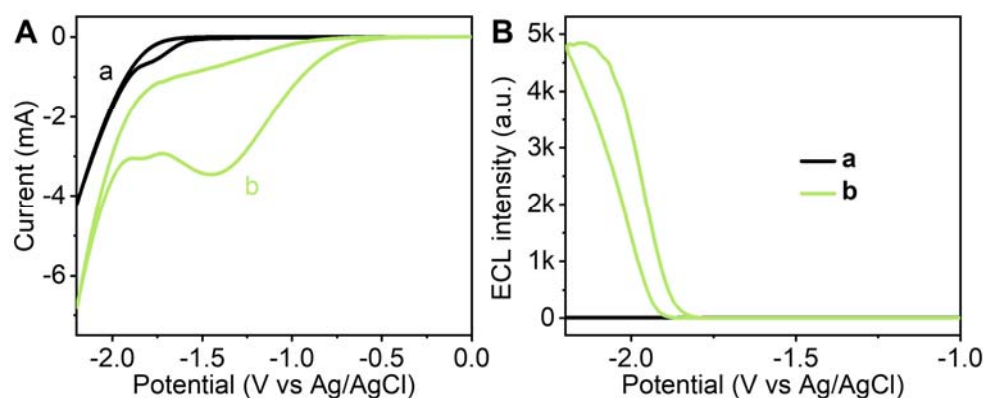
Fig. S27 (A) CV and (B) cathodic ECL curves of Mg-MOF modified GCEs in 0.1 M PBS without (a) and with (b) 0.1 M $K_2S_2O_8$ (PMT = 250 V).
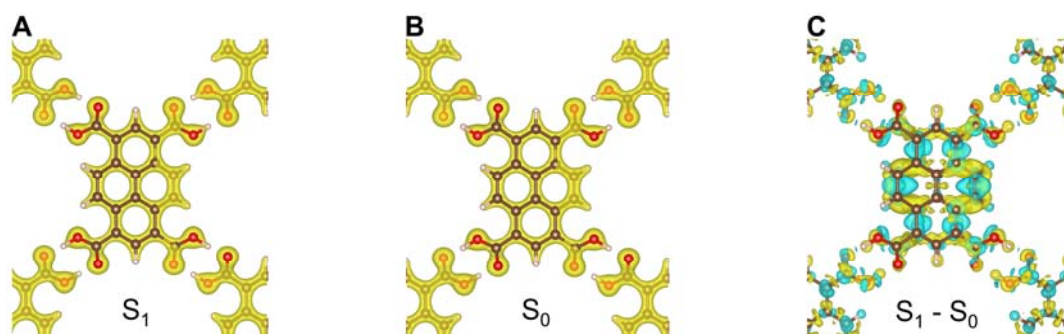
Fig. S28 The distribution profiles of charge density of (A) 1st excited state, (B) ground state, and (C) their difference for HOF-100 in top view (isosurface value = 0.0003 e bohr^{-3}).
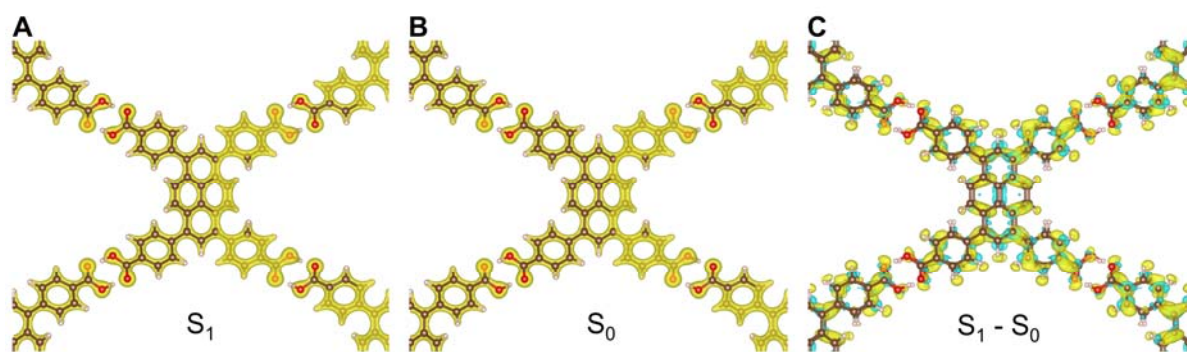
Fig. S29 The distribution profiles of charge density of (A) 1st excited state, (B) ground state, and (C) their difference for HOF-101 in top view (isosurface value = 0.0003 e bohr^{-3}).
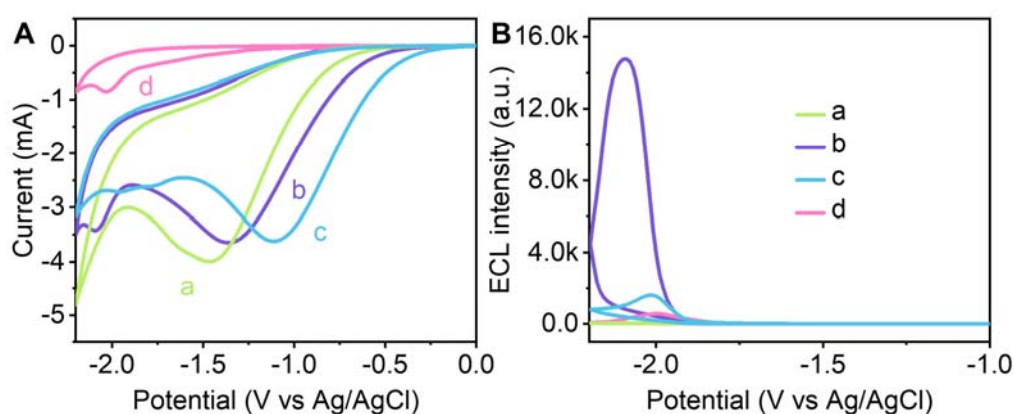
Fig. S30 (A) CV and (B) cathodic ECL curves of bare GCE (a), and HOF-101 (b) and TCPPY (c) modified GCEs in 0.1 M PBS with 0.1 M $K_2S_2O_8$, and (d) HOF-101 modified GCE without $K_2S_2O_8$ (PMT = 250 V).
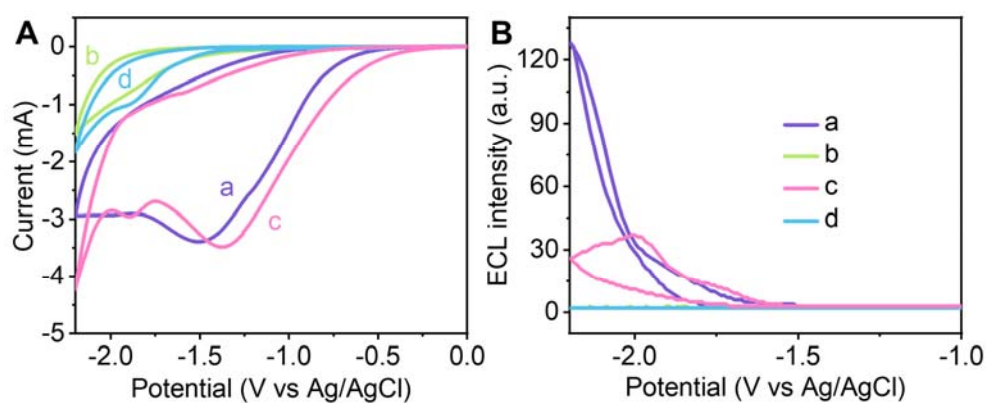
Fig. S31 (A) CV and (B) cathodic ECL curves of HOF-100 (a, b) and TCPY (c, d) modified GCEs in 0.1 M PBS with (a, c) and without (b, d) 0.1 M $K_2S_2O_8$ (PMT = 250 V).
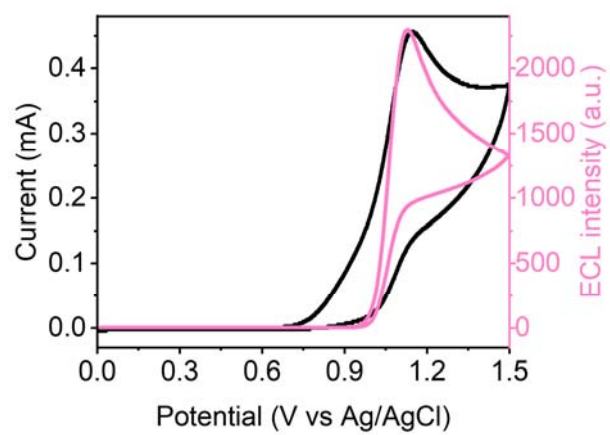
Fig. S32 CV (black) and anodic ECL (pink) curves of 0.1 mM Ru(bpy)$_3$Cl$_2$ in 0.1 M PBS containing 20 mM TPrA (PMT = 250 V).

Supporting Tables

Table S1. Experimental and computed band gaps, VBM, and CBM for HOF-101, TCPPY, HOF-100 and TCPY.

	TCPPY		HOF-101
	Experimental value (eV)	Computed value (eV)	Computed value (eV)
VBM	-5.54	-5.68	-5.54
CBM	-3.01	-3.05	-3.22
gap	2.53	2.63	2.32
	TCPY		HOF-100
	Experimental value (eV)	Computed value (eV)	Computed value (eV)
VBM	-6.55	-6.33	-7.23
CBM	-4.01	-3.53	-4.75
gap	2.54	2.80	2.48

Table S2. PL lifetimes of TCPY, HOF-100, TCPPY and HOF-101.

Solid	τ_1 (ns)	Rel (%)	τ_2 (ns)	Rel (%)
TCPY	1.02	45	7.83	55
HOF-100	0.68	73	4.81	27
TCPPY	2.58	48	13.94	52
HOF-101	2.72	74	7.90	26

Table S3. The electron effective mass transmitted out-of-plane of HOF-101 and HOF-100.

Out-of-plane	Electron effective mass (m_e^*/m_0)
HOF-101	1.49
HOF-100	2.07

Table S4. The calculated vertical excitation energies of TCPY, TCPPY, HOF-100 and HOF-101 fragments (isovalue = 0.02 e bohr^{-3}).

	Excited states	f	Calc. (nm)	Excited energy (eV)
	S_1	0.55	396.39	3.13
	S_2	0.03	369.39	3.36
	S_3	0.00	338.05	3.67
TCPY	T_1	0.00	966.73	1.28
	T_2	0.01	882.26	1.41
	T_3	0.01	701.67	1.77
	S_1	0.84	428.58	2.89
TCPPY	S_2	0.03	367.38	3.37
	S_3	0.00	354.26	3.50
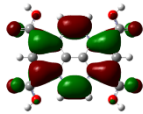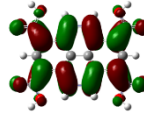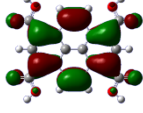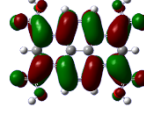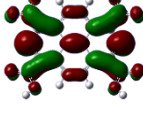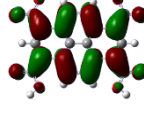
	State			
	T_1	0.08	839.09	1.48
	T_2	0.00	830.16	1.49
	T_3	0.09	752.80	1.65
	S_1	0.00	471.06	2.63
	S_2	0.00	458.18	2.71
HOF-100	S_3	0.00	406.87	3.05
	T_1	0.00	-4090.67	-0.30
	T_2	0.00	1211.79	1.02
	T_3	0.17	1148.52	1.08
	S_1	0.00	509.78	2.43
	S_2	0.00	499.33	2.48
HOF-101	S_3	0.00	470.36	2.64
	T_1	0.00	2207.75	0.56
	T_2	0.00	2098.86	0.59
	T_3	0.03	1095.36	1.13

Table S5. TDDFT calculation results of HOF-100 and HOF-101 fragments.

	State	Transition	Participating MO[a]	Transition character[b]
HOF-100	S_1	194	H → L (87.29%)	LE
		193	H -1 → L + 1 (12.39%)	LE
HOF-101	S_1	354	H → L +1 (92.13%)	LE
		353	H-1 → L (7.23%)	LE

[a] Orbital transition contribution value. [b] Local excitation (LE).

Table S6. Natural transition orbital (NTO) isodensity surfaces in S_0, S_1 and T_1. (isovalue = 0.02 e bohr^{-3}). Red and green regions denote the positive and negative orbital phases, respectively.

	Excited States		NTO		
TCPY	S_0	97		98	
	S_1	97		98	
	T_1	96B		97B	

TCPPY	S_0	177		178
	S_1	177		178
	T_1	178A		179A
HOF-100 fragment	S_0	194		195
	S_1	194		195
	T_1	194		195
HOF-101 fragment	S_0	354		355
	S_1	354		355
	T_1	354		355
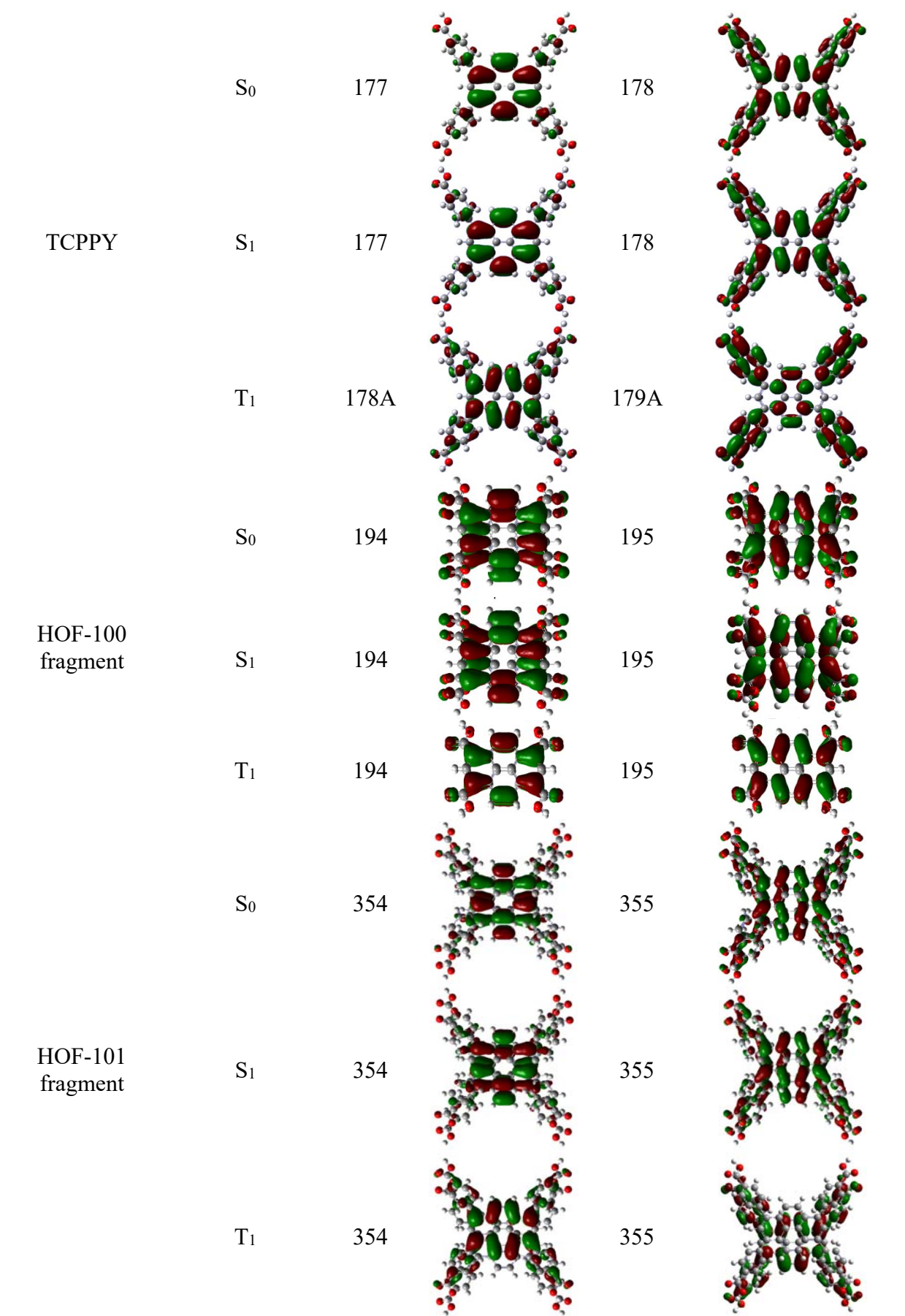
Table S7. Comparison of the Φ_{ECL} of different ECL emitters.

ECL emitters	Coreactants	Φ_{ECL} (%)	References
TPA-TBTN-COF	Dissolved oxygen	31.20	12
DAFB-TBTN-COF	Dissolved oxygen	57.10	13
DAFB-DCTP-COF	Dissolved oxygen	32.50	14
TPB NCs	TEA	31.53	15
Ox-Met-AuNCs	TEA	66.10	16
SS-ATT-AuNCs	TEA	78.00	17
Cd-In-S NCs	TPrA	2.10	18
CN-PPV Pdots	TPrA	11.22	19
BF$_2$ formazanate dye	TPrA	17.50	20
t-COF	TPrA	0.23	21
Tr-HOFs	TPrA	21.30	22
BN QDs	$K_2S_2O_8$	1.04	23
NAC-AuNCs	$K_2S_2O_8$	4.11	24
Py-sp^{2}c-COF	$K_2S_2O_8$	6.89	25
HHTP-HATP-COF	$K_2S_2O_8$	5.22	26
Zn-PTC	$K_2S_2O_8$	15.98	27
HOF-101	$K_2S_2O_8$	64.70	This work

¹H-NMR Spectroscopy

HOF-101   400 MHz, DMSO-d₆
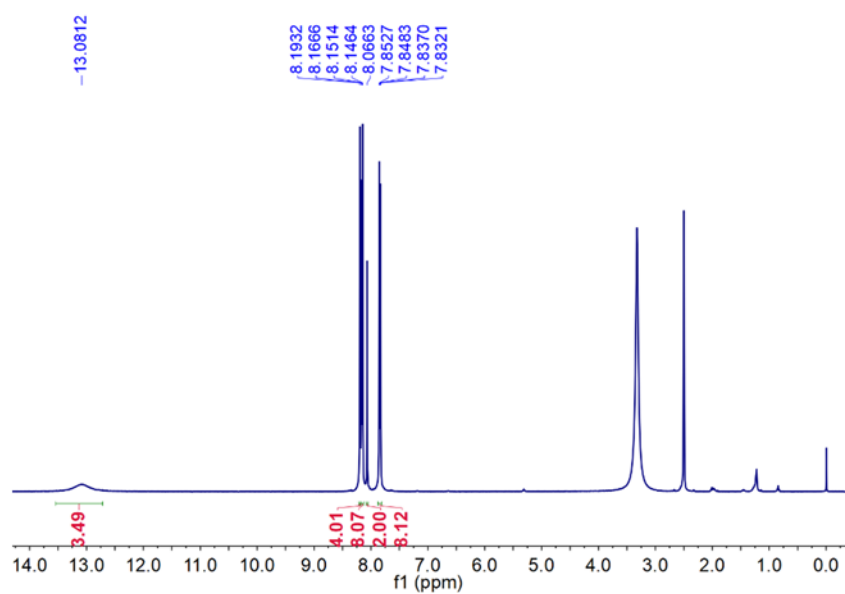
HOF-100   400 MHz, DMSO-d₆
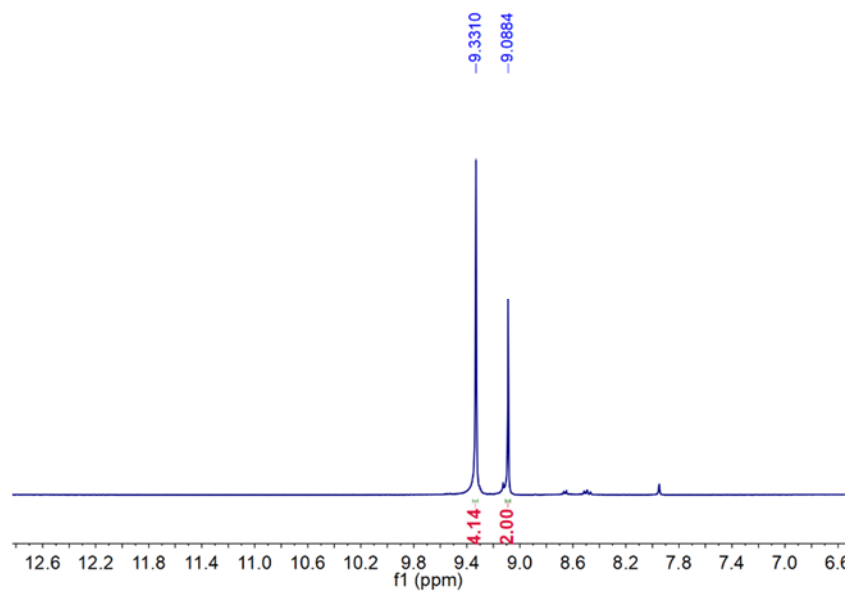
REFERENCES

1. Z. Hu, C. Qiao, Z. Xia, F. Li, J. Han, Q. Wei, Q. Yang, G. Xie, S. Chen and S. Gao, *ACS Appl. Mater. Interfaces*, 2020, **12**, 14914–14923.

2. G. Kresse and J. Furthmüller, *Phys. Rev. B*, 1996, **54**, 11169–11186.

3. G. Kresse and J. Furthmüller, *Comp. Mater. Sci.*, 1996, **6**, 15–50.

4. G. Kresse and D. Joubert, *Phys. Rev. B*, 1999, **59**, 1758–1775.

5. P. E. Blöchl, *Phys. Rev. B*, 1994, **50**, 17953–17979.

6. J. P. Perdew, K. Burke and M. Ernzerhof, *Phys. Rev. Lett.*, 1996, **77**, 3865–3868.

7. J. Heyd, G. E. Scuseria and M. Ernzerhof, *J. Chem. Phys.*, 2003, **118**, 8207–8215.

8. J. Paier, M. Marsman, K. Hummer, G. Kresse, I. C. Gerber and J. G. Ángyán, *J. Chem. Phys.*, 2006, **124**, 154709.

9. H. J. Monkhorst and J. D. Pack, *Phys. Rev. B*, 1976, **13**, 5188–5192.

10. M. Frisch, G. Trucks, H. Schlegel, G. Scuseria, M. Robb, J. Cheeseman, G. Scalmani, V. Barone, G. Petersson and H. Nakatsuji, Gaussian 16. Gaussian, Inc. Wallingford, CT: 2016.

11. A. D. Becke, *Phys. Rev. A*, 1988, **38**, 3098–3100.

12. Y.-J. Li, W.-R. Cui, Q.-Q. Jiang, R.-P. Liang, X.-J. Li, Q. Wu, Q.-X. Luo, J. W. Liu and J.-D. Qiu, *ACS Appl. Mater. Interfaces*, 2021, **13**, 47921−47931.

13. W.-R. Cui, Y.-J. Li, Q.-Q. Jiang, Q. Wu, Q.-X. Luo, L. Zhang, R.-P. Liang and J.-D. Qiu, *Anal. Chem.*, 2021, **93**, 16149−16157.

14. Y.-J. Li, W.-R. Cui, Q.-Q. Jiang, Q.-Wu, R.-P. Liang, Q.-X. Luo and J.-D. Qiu, *Nat. Commun.*, 2021, **12**, 4735.

15. J.-L. Liu, J.-Q. Zhang, Y. Zhou, D.-R. Xiao, Y. Zhuo, Y.-Q. Chai and R. Yuan, *Anal. Chem.*, 2021, **93**, 10890–10897.

16. H. Peng, Z. Huang, Y. Sheng, X. Zhang, H. Deng, W. Chen and J. Liu, *Angew. Chem., Int. Ed.*, 2019, **58**, 11691–11694.

17. H. Peng, Z. Huang, H. Deng, W. Wu, K. Huang, Z. Li, W. Chen and J. Liu, *Angew. Chem., Int. Ed.*, 2020, **59**, 9982–9985.

18. F. Wang, J. Lin, T. Zhao, D. Hu, T. Wu and Y. Liu, *J. Am. Chem. Soc.*, 2016, **138**, 7718–7724.

19. Y. Feng, N. Wang and H. Ju, *Anal. Chem.*, 2018, **90**, 1202–1208.

20. R. R. Maar, R. Zhang, D. G. Stephens, Z. Ding and J. B. Gilroy, *Angew. Chem., Int. Ed.*, 2019, **58**, 1052–1056.

21. R. Luo, H. Lv, Q. Liao, N. Wang, J. Yang, Y. Li, K. Xi, X. Wu, H. Ju and J. Lei, *Nat. Commun.*, 2021, **12**, 6808.

22. N. Zhang, X.-T. Wang, Z. Xiong, L.-Y. Huang, Y. Jin, A.-J. Wang, P.-X. Yuan, Y.-B. He and J.-J. Feng, *Anal. Chem.*, 2021, **93**, 17110–17118.

23. Y. Liu, M. Wang, Y. Nie, Q. Zhang and Q. Ma, *Anal. Chem.*, 2019, **91**, 6250–6258.

24. H. Peng, M. Jian, H. Deng, W. Wang, Z. Huang, K. Huang, A. Liu and W. Chen, *ACS Appl. Mater. Interfaces*, 2017, **9**, 14929–14934.

25. J.-L. Zhang, Y. Yang, W.-B. Liang, L.-Y. Yao, R. Yuan and D.-R. Xiao, *Anal. Chem.*, 2021, **93**, 3258–3265.

26. J.-L. Zhang, L.-Y. Yao, Y. Yang, W.-B. Liang, R. Yuan and D.-R. Xiao, *Anal. Chem.*, 2022, **94**, 3685–3692.

27. J.-M. Wang, L.-Y. Yao, W. Huang, Y. Yang, W.-B. Liang, R. Yuan and D.-R. Xiao, *ACS Appl. Mater. Interfaces*, 2021, **13**, 44079–44085.